

# Cumulative error correction of inertial navigation systems using LIDAR sensors and extended Kalman filter

Silmi Ath Thahirah Al Azhima<sup>1</sup>, Dadang Lukman Hakim<sup>2</sup>, Robby Ikhfa Nulfatwa<sup>3</sup>,  
Nurul Fahmi Arief Hakim<sup>1</sup>, Mariya Al Qibtiya<sup>1</sup>

<sup>1</sup>Industrial Automation and Robotic Education Study Program, Faculty of Technology and Vocational Education,  
Universitas Pendidikan Indonesia, Bandung, Indonesia

<sup>2</sup>Electrical Engineering Study Program, Faculty of Technology and Vocational Education, Universitas Pendidikan Indonesia,  
Bandung, Indonesia

<sup>3</sup>Electrical Engineering of Education Study Program, Faculty of Technology and Vocational Education,  
Universitas Pendidikan Indonesia, Bandung, Indonesia

---

## Article Info

### Article history:

Received Oct 3, 2023

Revised Feb 9, 2024

Accepted Feb 26, 2024

---

### Keywords:

Extended Kalman filter

LIDAR

Localization

Robotic

Wheel odometer

---

## ABSTRACT

Autonomous robots have gained significant attention in research due to their ability to facilitate human work. Navigation systems, particularly localization, present a challenge in autonomous robots. The inertial navigation system is a localization system that uses inertial sensors and a wheel odometer to estimate the robot's relative position to the initial position. However, the system is susceptible to continuous error accumulation over time due to factors like sensor noise and wheel slip. To address these issues, external sensors are required to measure the robot's position in the environment. The extended Kalman filter (EKF) method is utilized to estimate the robot's position based on wheel odometer and light detection and ranging (LIDAR) sensor measurements. In the prediction stage, the input to the EKF is the position measurement from the wheel odometer, while the LIDAR sensor's position measurement is used in the update stage to improve the prediction stage results. The test results reveal that the EKF's estimated position has a lower average error compared to the position measurement using the wheel odometer. Therefore, it can be concluded that the EKF technique is effectively applied to the robot and can correct the wheel odometer's cumulative error with the assistance of the LIDAR sensor.

*This is an open access article under the [CC BY-SA](https://creativecommons.org/licenses/by-sa/4.0/) license.*



---

## Corresponding Author:

Dadang Lukman Hakim

Electrical Engineering Study Program, Faculty of Technology and Vocational Education

Universitas Pendidikan Indonesia

Setiabudi Street, Bandung, West Java 40162, Indonesia

Email: dadanglh@upi.edu

---

## 1. INTRODUCTION

The rapid advancement of technology has led to a significant increase in the development of mobile autonomous robots. One crucial aspect of these robots is navigation, which remains a widely studied subject due to various obstacles, such as robot localization or positioning. Precise localization of navigation systems in autonomous robots is vital for their accurate and efficient task performance. Numerous research studies have focused on addressing the challenges of mobile robot localization and navigation, including path-planning strategies, probabilistic approaches, and evolutionary approaches [1]–[3]. Another research area that poses a challenge is the planning and control of autonomous mobile robots for intralogistics [4]. Achieving successful navigation relies on excelling in four key components: locomotion, perception, cognition, and

navigation [5]. The challenges in the field of robotics encompass navigating unexplored environments, controlling multiple diverse robots, adapting coordination, interfacing, and utilizing multiple resources, as well as sharing information from various data sources with varying reliability and accuracy.

There are limitations related to the utilization of error correction in the extended Kalman filter (EKF) algorithm when applied to multi-sensor localization models. Error rectification is a distributed process, which increases the system's vulnerability to sensor failure. Errors propagating from a single sensor can impact the entire network. Furthermore, careful design considerations are necessary due to the complexity associated with the implementation and maintenance of a distributed error correction mechanism for the EKF algorithm [6]. Adaptive fuzzy EKF-based inertial navigation system (INS) and global positioning systems (GPS) sensor fusion is a potent method for enhancing navigation precision through the integration of data from INS and GPS sensors. Nevertheless, its primary drawback is its susceptibility to interference, which presents challenges in environments that are dynamic and unpredictable. Adaptive fuzzy EKFs encounter challenges in promptly adjusting their parameters to dynamic conditions, which may result in inadequate performance in the face of unforeseen disruptions. Difficulties exist in precisely characterizing disturbances, and imprecise EKF estimation errors may result from the sensitivity of these disturbances to alterations in the navigation state. Due to the close connection between the efficiency of the EKF method and the adjustment of fuzzy logic parameters, it is necessary to exercise caution and make appropriate adjustments to guarantee optimal performance amidst disturbances [7]. Certain drawbacks are associated with the comparison between the EKF and silicon artificial neural network (Si-ANN) for sensorless speed control of DC motors. An essential constraint of Si-ANN is its reliance on training data sets, which are notoriously challenging to acquire and impede the accurate recognition of intricate motor movements. The operational parameters of the DC motor and the caliber of the training data have a substantial impact on the performance of Si-ANN. When deciding between EKF and Si-ANN for sensorless speed control, application-specific requirements, trade-offs between computational complexity and accuracy, and the method's adaptability to dynamic and changing operating conditions must all be carefully considered. The implementation of EKF and Si-ANN for sensorless speed regulation of a DC motor [8].

The use of modeling in the EKF process includes kinematic and dynamic models [9], [10]. Kinematic models represent movement without considering the causes of that movement, while dynamic models take into account the forces acting on the system. A study presented a motion-predictive EKF for autonomous underwater vehicles (AUVs) using a simplified dynamic model, which showed good prediction accuracy for the dynamic filter [11]. Another study proposed a modified kinematic model for track geometry based on tangential and normal curves [12]. The design and configuration of the automaton employed have no bearing on the kinematic model, allowing for a more straightforward description of motion. Kinematic modeling is a versatile tool for describing movement because it is not dependent on the particular shape or class of the robot. This assertion finds support in robotics research, which has effectively implemented kinematic models across diverse robot configurations and type, such as continuum robots, skid-steered mobile robots, and track geometries [13], [14]. As a result, the kinematic model remains unaffected by the particular attributes of the robot's form or category, enabling it to furnish a comprehensive and readily implementable depiction of motion.

This study investigated the effects of navigation system utilizing the EKF method with a nonlinear model derived from the kinematic model. EKF has an advantage in terms of accuracy. So, it is suitable for 3-wheeled omni-directional. The objective is to achieve efficient computation and independence from the specific type or configuration of the robot employed. The system is intended for implementation on a 3-wheeled omni-directional robot operating with a kinematic model featuring 2 degrees of freedom (DoF). With this model, the navigation system remains viable even if alterations are made to the robot's type or configuration. The study investigates error correction techniques to rectify cumulative errors in wheel odometry within an inertial navigation system, utilizing light detection and ranging (LIDAR) sensors and EKF localization in the context of three omni-directional robotics. The robot, shaped like an equilateral triangle, is outfitted with an omni drive wheel, enabling movement in any direction within a 2-dimensional plane. The methodology involves the integration of wheel odometry and LIDAR sensor data through the EKF method. Two sets of odometric data, obtained from the wheel odometry and LIDAR sensor, are utilized. The experiment concentrates on localizing the robot's position and orientation along the  $x$ ,  $y$ , and  $\theta$  axes.

## 2. THE PROPOSED METHOD

The necessary mechanical system for the robot is a wheelbase designed to house the propulsion system and offer ample dimensions for accommodating other systems. The wheelbase, of the three-omni wheel type, features a wheel configuration with an angle of 120 degrees between them. The block diagram illustrating the interconnections among robot systems is depicted in Figure 1. The initial step preceding the design process involves conducting an analysis of system requirements. This analysis encompasses various

facets, such as localization systems, drive systems, hardware systems, and mechanical systems. To determine the robot's position accurately, it is imperative to utilize sensors capable of providing precise position data. In this study, positioning is accomplished through the incorporation of two types of sensors: internal sensors and external sensors. The internal sensor utilized to measure the robot's movement towards its initial position is the rotary encoder integrated within the DC motor. In contrast, the external sensor employed is LIDAR, which measures the distance between the robot and its surrounding environment. This system is composed of multiple printed circuit boards (PCBs), including a main PCB housing the primary microcontroller, a DC motor driver PCB, and a rotary encoder PCB.

The block diagram depicting the robot localization system utilizing wheel odometry and LIDAR sensors is presented in Figure 2. These two types of sensors yield robot position data in the form of odometry, specifically data for  $x$ ,  $y$ , and  $\theta$ . To enhance accuracy, the EKF method is employed to combine and process the two sets of data, resulting in a more precise position estimate.

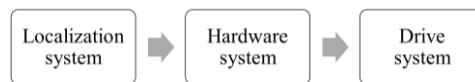


Figure 1. Robot system block diagram

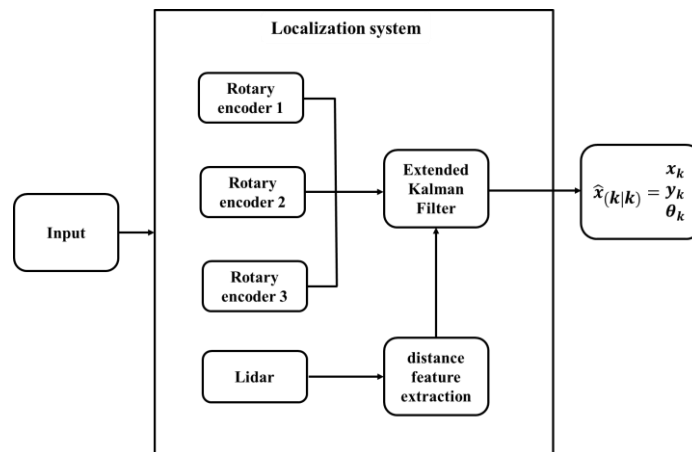


Figure 2. Block diagram of localization system

The illustration of the EKF algorithm is presented in Figure 3. By employing the EKF filter for position estimation, the cumulative error generated by the wheel odometer is intended to be corrected. To ascertain the location of the robot with respect to its environment, an external sensor is indispensable; this sensor happens to be the LIDAR. In the prediction phase, the EKF estimates the robot's location at time  $k$  utilizing odometry data obtained from the wheel odometer. During the correction phase, the odometric data acquired from LIDAR is subsequently integrated into the EKF in an effort to improve the results achieved in the prediction phase that came before it. At time  $k+1$ , the input to the prognosis stage is the final result obtained during the correction phase. The Kalman filter (KF) is a technique utilized to estimate a value, specifically the linear least mean squares estimator (LLSME). It improves system performance by utilizing the statistical properties of noise and an accurate dynamic model of the system [15]. The EKF is a derivative of the KF designed to estimate the state of the system. On the contrary, the KF is regarded as the most effective linear estimator in cases where the noise that impacts both the process and the measurements has a white gaussian distribution. It is imperative to emphasize that the KF is solely applicable in situations where a linear equation can represent the state space model, specifically the state transition function. This suggests that the temporal progression of the system's state can be represented graphically as a linear trend [16]. The EKF determines the state of the system by means of a feedback-integrated control mechanism. Typically, the EKF algorithm is divided into prediction and update phases. The prediction stage involves the utilization of control input to forecast the state of the system, as well as the covariance matrix [17], [18]. In order to adjust the state of the system, the Kalman gain is computed during the correction phase. A comprehensive explanation of the EKF algorithm for each process will be provided in Figure 3.

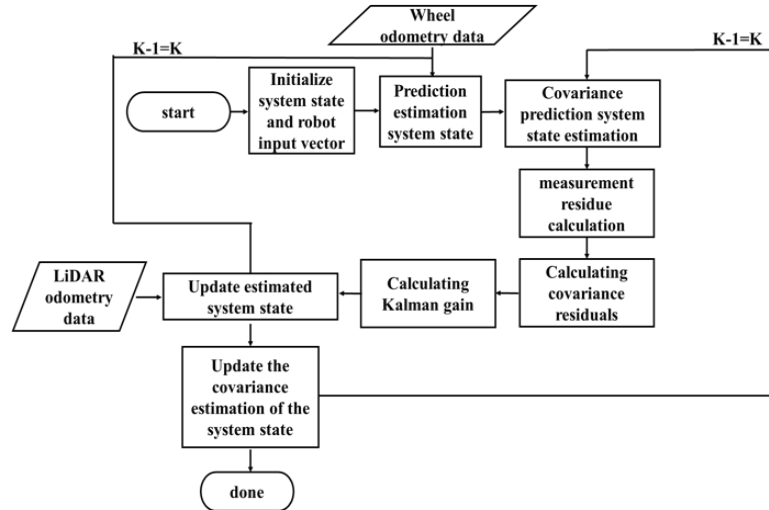


Figure 3. Estimation algorithm flow chart with EKF

**2.1. Initialization**

Initialization is a prerequisite for the establishment of the initial value of the system state during the initial phase of the EKF procedure. Initialization for the initial state occurs at the preceding time, specifically  $k-1$ , assuming the current time is denoted by  $g$ . Given that the robot is initially situated at coordinates  $(0, 0)$ . In addition to the state of the system, the input vector values are required to initiate the EKF during the initial iteration. In the absence of any input at this time, the input vector is specified using (1) and (2) [19].

$$\hat{x}_{k-1|k-1} = \begin{bmatrix} x_{k-1} \\ y_{k-1} \\ \theta_{k-1} \end{bmatrix} = \begin{bmatrix} 0 \\ 0 \\ 0 \end{bmatrix} \tag{1}$$

$$u_{k-1} = \begin{bmatrix} u_{k-1} \\ w_{k-1} \end{bmatrix} = \begin{bmatrix} 0 \\ 0 \end{bmatrix} \tag{2}$$

**2.2. System state estimation prediction**

During this phase, it is essential to employ a state space model to forecast the system’s state at time  $k$ , considering the state of the system and the input vector at the previous time  $k-1$ . The state space model equation for this purpose is represented by (3) [20]. Where  $\hat{x}_{k|k-1}$  is system state prediction estimation.  $A_{k-1}$  is represents the change in the system at time  $k-1$  when no input vector is given.  $x_{k-1}$  is the state vector of the system at  $k-1$ .  $B_{k-1}$  is system changes when given an input vector.  $u_{k-1}$  is input vector. And  $v_{k-1}$  is noise.

$$\hat{x}_{k|k-1} = A_{k-1}x_{k-1} + B_{k-1}u_{k-1} + v_{k-1} \tag{3}$$

**2.3. Covariance prediction from system state estimation**

In practical implementation, the EKF is used to estimate the state and state estimation error covariance values from real-time data [21]. Because the predictions from the estimation of the previous state of the system are not 100% accurate, we need a matrix  $P_{k|k-1}$  which represents the accuracy of these predictions using (4). Where  $P_{k|k-1}$  is prediction of the covariance matrix.  $F_k$  is matrix A in the equation state space models.  $F_k^T$  is transpose matrix of  $F_k$ .  $P_{k-1|k-1}$  is covariance matrix at  $k-1$ .  $Q_k$  is the matrix that represents confidence in sensor measurement predictions.

$$P_{(k|k-1)} = F_k P_{k-1|k-1} F_k^T + Q_k \tag{4}$$

**2.4. Residue measurement**

The residue measurement in the EKF is addressed through the measurement update equations, which correct the state and covariance estimates using sensor measurements, measurement Jacobians, and measurement noise covariance [22], [23]. The measurement residue is the difference between the sensor’s actual observations and the sensor’s predicted observations. Residual measurements can be calculated using (5). Where  $\bar{y}_k$  is measurement residue.  $z_k$  is sensor measurement matrix.  $h(x_{k|k-1})$  is observation model.

$$\bar{y}_k = z_k - h(x_{(k|k-1)}) \quad (5)$$

### 2.5. Covariant residues

Residual covariance is a matrix that represents the residuals from the covariance predictions of system measurements. The residual covariance can be calculated using (6). Where  $S_k$  is covariant residue.  $H_k$  is measurement matrix.  $H_k^T$  is matrix transpose of matrix measurement.  $R_k$  is sensor noise covariance matrix measurement.

$$S_k = H_k P(k|k-1) H_k^T + R_k \quad (6)$$

### 2.6. Kalman gain

This value indicates how much the prediction of the state of the system and the prediction of the covariance of the correction for the new state of the system are. Kalman gain ( $K_k$ ) can be calculated from several components that have been obtained previously using (7). Such as covariance prediction ( $P_{k|k-1}$ ), transpose measurement matrix  $H_k^T$ , and inverse covariance residual matrix ( $S_{k-1}$ ).

$$K_k = P(k|k-1) H_k^T S_k^{-1} \quad (7)$$

### 2.7. System state estimation update

The EKF, which is a nonlinear full-state estimator given the sensor measurements, the model prediction, and their variances, approximates the state estimate with the smallest covariance error. The calculation of the final estimate of EKF is possible via (8). The estimation of the system's current state is revised each time a new sensor measurement is acquired.

$$\hat{x}(k|k) = \hat{x}(k|k-1) + K_k \bar{y}_k \quad (8)$$

### 2.8. System state covariance estimation update

The system state covariance estimation update in the EKF aims to continuously refine the covariance matrix, providing a more accurate depiction of the uncertainty in the system's state variables as new measurements are incorporated into the filtering process [24], [25]. In addition to the state estimation, the output of the EKF system is the estimation of the system state covariance using (9). The refined state variables  $\hat{x}(k|k)$  and  $P(k|k)$  will be used for predictions in the next iteration. The process of the EKF stages is carried out repeatedly as many iterations as needed.

$$P(k|k) = (I - K_k H_k) P(k|k-1) \quad (9)$$

## 3. RESULTS AND DISCUSSION

### 3.1. System design

During this phase, the design of the robot's mechanical system is developed, taking into account the previously conducted needs analysis. The outcome of the design is an equilateral triangle-shaped robot with a length of 476.54 mm. The robot mechanical system is designed to be made using acrylic material with a thickness of 5 mm for layer 1 and 2 mm for layer 2, see in Figure 4. The bottom layer 1 functions as a wheelbase or seat for omni wheels and DC motors. Meanwhile, on layer 1, the upper part functions as a place for the hardware system. Layer 2 is used as a place to store LIDAR sensors.

The hardware system created functions to integrate robot components. The block diagram of the hardware system is shown in Figure 5. The STM32F767ZI microcontroller functions to process all inputs, both from the control system and from sensors, into outputs in the form of robotic actions. The input and output components processed by the controller are the rotary encoder, LIDAR, and the BTS7690 motor driver. At the component input, the rotary encoder is connected to a digital pin. While LIDAR is connected using serial communication pins Rx and Tx. As for the output component, the BTS7690 is connected to a digital pin which is set as pulse width modulation (PWM) so that the motor speed can be adjusted. In order for the robot to move in an omni directional manner or in all directions, a drive called an omni wheel or omni wheel is required. The omni wheel component has the ability to move on the x and y axes. The omni wheel is connected to a PG45 DC motor using a hub that is adjusted to the hole between the wheel and the motor.

Three omni wheels are used because the robot's triangular design. Each omni wheel drive motor is controlled by a motor driver, namely the BTS7690 which is connected to the STM32F767ZI.

The flowchart of robot positioning using the odometry method is shown in Figure 6. The odometry system is designed using three rotary encoder sensors installed in the PG45 DC motor. This sensor has 2 input channels with an output pulse of 7 ppr. The rotary encoder is mounted on an omni wheel with a diameter of 12 cm with a three omni-directional configuration. With this configuration, position data of  $x$ ,  $y$ , and  $\theta$  of the robot can be obtained using the odometry method.

The positioning algorithm using the LIDAR sensor can be seen in Figure 7. LIDAR is an object detection method that uses the principle of laser light reflection to measure the distance of objects on the earth's surface. The sensor used on the robot is RPLIDAR A1M8 which has specifications that can detect distances of up to 12 meters. In this study, the sensor is used to determine the position with a reference to the initial position.

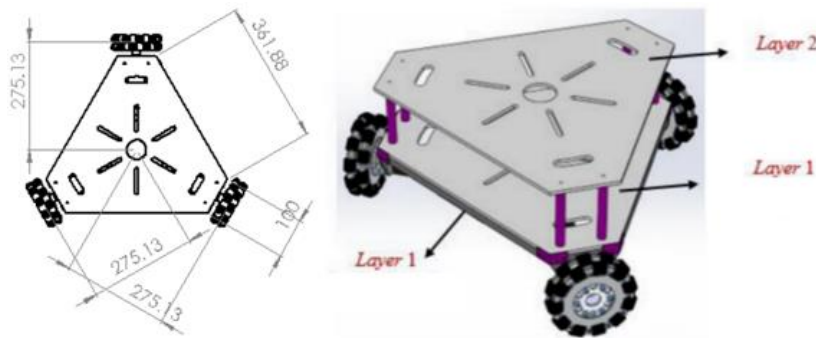


Figure 4. Dimension of omni-directional robot

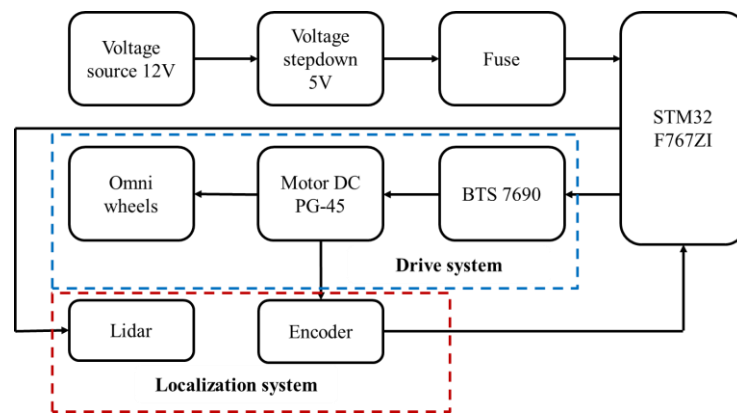


Figure 5. Block diagram of the hardware system

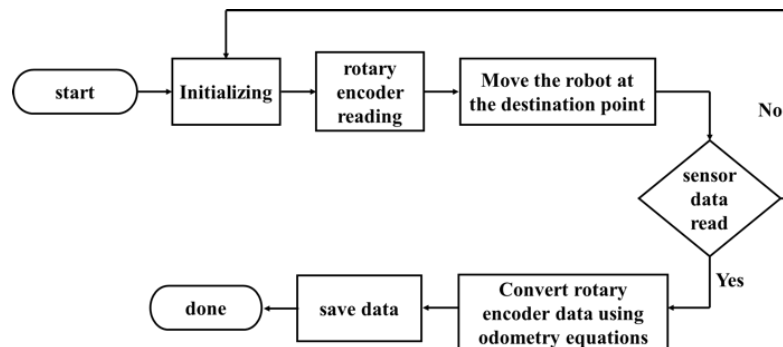


Figure 6. Robot positioning flowchart

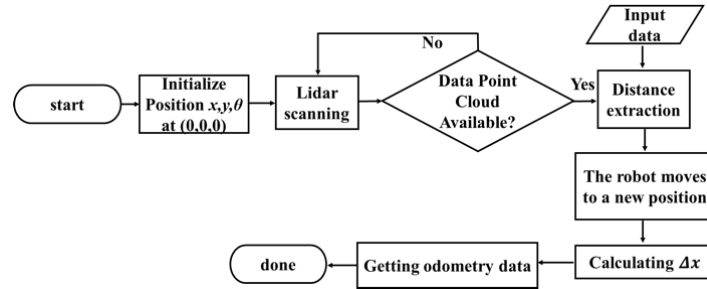


Figure 7. Flowchart of positioning algorithm using LIDAR sensor

In EKF, two models are required from the robots, specifically the state space model and the observation model. In this study, the robot moves on a flat plane, and the state of the robot is defined by matrix (10). Since the robot moves omnidirectionally, the control signal  $u$  is defined as the vector of position and orientation velocities, as depicted in Figure 8. Thus, the control signal can be described by (11) [26].

$$X = \begin{bmatrix} x \\ y \\ \theta \end{bmatrix} \quad (10)$$

$$u = \begin{bmatrix} v_x \\ v_y \\ v_\theta \end{bmatrix} \quad (11)$$

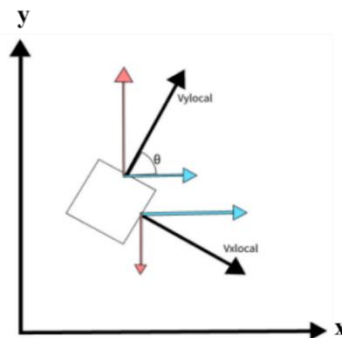


Figure 8. Vector illustration of speed positioning and orientation of a robot

### 3.2. System testing

The objective of the wheel odometry localization test is to assess the error value in data acquisition. The test procedure involves positioning the robot at coordinates (0,0) and subsequently moving it to the subsequent point. The test findings indicate an average error of 189.9 mm along the X-axis and 129.8 mm along the Y-axis, as presented in Table 1 of the odometry localization test data. Position measurement testing using a LIDAR sensor. The method for this sensor is to measure the distance from the object to the surface so that two wall planes are used. The results obtained are the average error value on the X and Y axes of 1.8 mm can be seen in Table 2.

The odometry sensor located on the omniwheel wheel serves as the primary sensor within this navigation system. In contrast, the measurements obtained from this odometry sensor exhibit a substantial margin of error. Consequently, an additional sensor with enhanced precision is required in order to rectify the resultant error. You can rectify odometry-induced errors in the navigation system by integrating LIDAR and odometry via sensor fusion utilizing the EKF method. Table 3 and Figure 9 illustrate that the error value associated with the EKF results is 2.26 for the X coordinates and 4.05 for the Y coordinates. Prior to and subsequent to the integration of odometry and LIDAR through EKF, the error value generated by odometry decreased by 187.54 in X coordinates and 125.3 in Y coordinates, respectively. As a result, it can be deduced that the LIDAR sensor effectively corrects errors in the omniwheel encoder sensor reading.

Table 1. Odometry localization data

Coordinate		Measured coordinates		Error	
X (mm)	Y (mm)	X (mm)	Y (mm)	X (mm)	Y (mm)
0	0	0	0	0	0
0	1,500	79	1,177	79	323
750	1,300	1,277	995	-527	305
750	200	1,174	152	-424	48
0	0	-81	27	81	-27
Error average (mm)				189.8	129.8

Table 2. LIDAR localization data

Coordinate		Measured coordinates		Error	
X (mm)	Y (mm)	X (mm)	Y (mm)	X (mm)	Y (mm)
0	0	-4	-7	4	7
0	1,500	13	1,502	-13	-2
750	1,300	756	1,320	-6	-20
750	200	735	183	15	17
0	0	-9	-7	9	7
Error average (mm)				1.8	1.8

Table 3. Comparison data

Coordinate		Odometry		LIDAR		EKF estimate	
X(mm)	Y(mm)	X(mm)	Y(mm)	X(mm)	Y(mm)	X(mm)	Y(mm)
0	0	0	0	-4	-7	-4.42	-7.72
0	1,500	79	1,177	13	1,502	19.75	1,465.95
750	1,300	1,277	995	756	1,320	710.77	1,323.56
750	200	1,174	152	735	183	721.3	213.96
0	0	-81	27	-9	-7	41.3	-16
Error average		189.8	129.8	1.8	1.8	2.26	4.05

The results of the analysis obtained from the experiment, included:

- i) The positioning accuracy achieved through wheel odometry exhibits significant errors, with 189.8 mm on the X-axis and 129.8 mm on the Y-axis. Therefore, there is a need for a method that can rectify these errors.
- ii) The LIDAR odometry approach results in identical error values of 1.8 mm on both the X-axis and Y-axis. Hence, the utilization of LIDAR sensors can effectively mitigate the errors originating from wheel odometry localization.
- iii) The position estimation obtained through the implementation of the EKF method yields an error of 2.26 mm on the X-axis and 4.05 mm on the Y-axis concerning the actual position. This demonstrates that the cumulative errors derived from wheel odometry localization can be effectively corrected by employing LIDAR sensors in conjunction with the EKF method.
- iv) The results obtained have quite high accuracy on omni-directional robots without taking into account the dynamic model of the robot. However, it is necessary to carry out deeper investigations into other forms of robots.

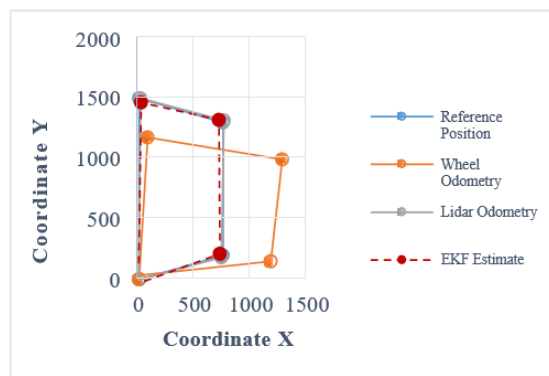


Figure 9. Graphic of comparison data



#### 4. CONCLUSION

Recent observations suggest that the inertial navigation system with positioning using a wheel odometer causes errors to accumulate continuously every time, causing positioning to be less accurate. To overcome this, the LIDAR sensor is used to correct the accumulative error of the wheel odometer by applying the EKF method. Odometry data from the wheel odometer is used to predict the robot's position and odometry data from the LIDAR sensor is used to update the data by entering some system noise. The error resulting from estimating the position of the EKF is smaller than measuring the position with the wheel odometer. So that the positioning system using the EKF with the LIDAR sensor was successfully implemented and resulted in a more accurate position estimation. Comparative research is one of the suggestions for additional study, which should consider whether the dynamic model of the robot will yield substantial performance improvements.

#### ACKNOWLEDGEMENTS

This work was supported by UPI research program under contract number 555/UN40.LP/PT.01.03/2023.




#### REFERENCES

- [1] F. Rubio, F. Valero, and C. Llopis-Albert, "A review of mobile robots: concepts, methods, theoretical framework, and applications," *International Journal of Advanced Robotic Systems*, vol. 16, no. 2, p. 172988141983959, Mar. 2019, doi: 10.1177/1729881419839596.
- [2] J. R. Sánchez-Ibáñez, C. J. Pérez-del-Pulgar, and A. García-Cerezo, "Path planning for autonomous mobile robots: a review," *Sensors*, vol. 21, no. 23, p. 7898, Nov. 2021, doi: 10.3390/s21237898.
- [3] P. K. Panigrahi and S. K. Bisoy, "Localization strategies for autonomous mobile robots: a review," *Journal of King Saud University - Computer and Information Sciences*, vol. 34, no. 8, pp. 6019–6039, Sep. 2022, doi: 10.1016/j.jksuci.2021.02.015.
- [4] G. Fragapane, R. de Koster, F. Sgarbossa, and J. O. Strandhagen, "Planning and control of autonomous mobile robots for intralogistics: literature review and research agenda," *European Journal of Operational Research*, vol. 294, no. 2, pp. 405–426, Oct. 2021, doi: 10.1016/j.ejor.2021.01.019.
- [5] D. Gorinevsky, S. Boyd, and G. Stein, "Design of low-bandwidth spatially distributed feedback," *IEEE Transactions on Automatic Control*, vol. 53, no. 1, pp. 257–272, Feb. 2008, doi: 10.1109/TAC.2007.914950.
- [6] F. Hu and G. Wu, "Distributed error correction of EKF algorithm in multi-sensor fusion localization model," *IEEE Access*, vol. 8, pp. 93211–93218, 2020, doi: 10.1109/ACCESS.2020.2995170.
- [7] D. Sabzevari and A. Chatraei, "INS/GPS sensor fusion based on adaptive fuzzy EKF with sensitivity to disturbances," *IET Radar, Sonar & Navigation*, vol. 15, no. 11, pp. 1535–1549, Nov. 2021, doi: 10.1049/rsn2.12144.
- [8] A. Gundogdu, R. Celikel, and O. Aydogmus, "Comparison of SI-ANN and extended kalman filter-based sensorless speed controls of a DC motor," *Arabian Journal for Science and Engineering*, vol. 46, no. 2, pp. 1241–1256, Feb. 2021, doi: 10.1007/s13369-020-05014-3.
- [9] A. Quraishi and A. Martinoli, "Online kinematic and dynamic parameter estimation for autonomous surface and underwater vehicles," in *2021 IEEE/RSJ International Conference on Intelligent Robots and Systems (IROS)*, Sep. 2021, pp. 4374–4381, doi: 10.1109/IROS51168.2021.9636659.
- [10] G. Wang, Z. Wang, B. Huang, Y. Gan, and F. Min, "Active compliance control based on EKF torque fusion for robot manipulators," *IEEE Robotics and Automation Letters*, vol. 8, no. 5, pp. 2668–2675, May 2023, doi: 10.1109/LRA.2023.3258697.
- [11] B. Allotta *et al.*, "A new AUV navigation system exploiting unscented Kalman filter," *Ocean Engineering*, vol. 113, pp. 121–132, Feb. 2016, doi: 10.1016/j.oceaneng.2015.12.058.
- [12] J. S. Lee, I. Y. Choi, S. Kim, and D. S. Moon, "Kinematic modeling of a track geometry using an unscented kalman filter," *Measurement*, vol. 94, pp. 707–716, Dec. 2016, doi: 10.1016/j.measurement.2016.09.016.
- [13] J. S. Lee, S. H. Hwang, I. Y. Choi, and Y. Choi, "Deterioration prediction of track geometry using periodic measurement data and incremental support vector regression model," *Journal of Transportation Engineering, Part A: Systems*, vol. 146, no. 1, Jan. 2020, doi: 10.1061/JTEPBS.0000291.
- [14] S. Dogru and L. Marques, "An improved kinematic model for skid-steered wheeled platforms," *Autonomous Robots*, vol. 45, no. 2, pp. 229–243, Feb. 2021, doi: 10.1007/s10514-020-09959-0.
- [15] Y.-W. Chen and K.-M. Tu, "Robust self-adaptive Kalman filter with application in target tracking," *Measurement and Control*, vol. 55, no. 9–10, pp. 935–944, Nov. 2022, doi: 10.1177/00202940221083548.
- [16] M. Fathi, N. Ghahramani, M. A. S. Ashtiani, A. Mohammadi, and M. Fallah, "Incremental predictive Kalman filter for alignment of inertial navigation system," in *Proceedings of the Institution of Mechanical Engineers, Part G: Journal of Aerospace Engineering*, Nov. 2018, p. 095441001879432, doi: 10.1177/0954410018794324.
- [17] D. A. De Souza *et al.*, "Identification by recursive least squares with Kalman filter (RLS-KF) applied to a robotic manipulator," *IEEE Access*, vol. 9, pp. 63779–63789, 2021, doi: 10.1109/ACCESS.2021.3074419.
- [18] J. P. L. Caña, J. García Herrero, and J. M. M. López, "Forecasting nonlinear systems with LSTM: analysis and comparison with EKF," *Sensors*, vol. 21, no. 5, p. 1805, Mar. 2021, doi: 10.3390/s21051805.
- [19] M. Faisal *et al.*, "Enhancement of mobile robot localization using extended Kalman filter," *Advances in Mechanical Engineering*, vol. 8, no. 11, p. 168781401668014, Nov. 2016, doi: 10.1177/1687814016680142.
- [20] C. H. Do and H.-Y. Lin, "Incorporating neuro-fuzzy with extended Kalman filter for simultaneous localization and mapping," *International Journal of Advanced Robotic Systems*, vol. 16, no. 5, Sep. 2019, doi: 10.1177/1729881419874645.
- [21] I. Ullah, X. Su, X. Zhang, and D. Choi, "Simultaneous localization and mapping based on Kalman filter and extended Kalman filter," *Wireless Communications and Mobile Computing*, vol. 2020, pp. 1–12, Jun. 2020, doi: 10.1155/2020/2138643.
- [22] Y. Deng, X. Hou, B. Li, J. Wang, and Y. Zhang, "A highly powerful calibration method for robotic smoothing system calibration via using adaptive residual extended Kalman filter," *Robotics and Computer-Integrated Manufacturing*, vol. 86, p. 102660, Apr. 2024, doi: 10.1016/j.rcim.2023.102660.




- [23] L. Xu and R. Niu, "EKFNet: learning system noise statistics from measurement data," in *ICASSP 2021 - 2021 IEEE International Conference on Acoustics, Speech and Signal Processing (ICASSP)*, Jun. 2021, pp. 4560–4564, doi: 10.1109/ICASSP39728.2021.9415083.
- [24] A. Maheshwari and S. Nageswari, "Effect of Noise covariance matrices on state of charge estimation using extended Kalman filter," *IETE Journal of Research*, pp. 1–12, Apr. 2022, doi: 10.1080/03772063.2022.2055657.
- [25] C. Muscas, P. A. Pegoraro, S. Sulis, M. Pau, F. Ponci, and A. Monti, "New Kalman filter approach exploiting frequency knowledge for accurate PMU-based power system state estimation," *IEEE Transactions on Instrumentation and Measurement*, vol. 69, no. 9, pp. 6713–6722, Sep. 2020, doi: 10.1109/TIM.2020.2977744.
- [26] D. Wang, H. Liang, T. Mei, H. Zhu, J. Fu, and X. Tao, "LIDAR scan matching EKF-SLAM using the differential model of vehicle motion," in *2013 IEEE Intelligent Vehicles Symposium (IV)*, Jun. 2013, pp. 908–912, doi: 10.1109/IVS.2013.6629582.

## BIOGRAPHIES OF AUTHORS






**Silmi Ath Thahirah Al Azhima**    received a Bachelor and Master Degree of Electrical Engineering majoring in control and intelligent system from Institut Teknologi Bandung in 2019. She currently serves as a lecturer at the Technology and Vocational Education Faculty, Universitas Pendidikan Indonesia, Bandung, Indonesia. She is involved in robotic field research and interest control, intelligent system, navigation system, and autonomous system. She can be contacted at email: silmithahirah@upi.edu.






**Dadang Lukman Hakim**    received a B.Ed. Bachelor of Electrical Engineering from Universitas Pendidikan Indonesia, Bandung, Indonesia, in 1992, a master's degree in electrical engineering is majoring in power electrical from Institut Teknologi Bandung, Indonesia, in 2003, and a doctorate of Education Administration from Universitas Pendidikan Indonesia, Bandung, Indonesia, in 2016. He currently serves as a lecturer at the Technology and Vocational Education Faculty, Universitas Pendidikan Indonesia, Bandung, Indonesia. He is involved in power electrical field research and interest control system and machine learning to use in power electrical. He can be contacted at email: dadanglh@upi.edu.






**Robby Ikhfa Nulfatwa**    is an enthusiastic undergraduate student pursuing a degree in Electrical Engineering Education at the Faculty of Technology and Vocational Education, Universitas Pendidikan Indonesia. With a specific focus on robotics research, he actively participates in various robot contests in Indonesia. His passion for innovation, coupled with his dedication to electrical engineering education, positions him as a driven and promising individual in the field. He can be contacted at email: robyin13@upi.edu.



**Nurul Fahmi Arief Hakim**    received a B.Ed. Bachelor of Electrical Engineering Education from the Indonesian Education University, Bandung, Indonesia, in 2014, and a master's degree in electrical engineering is majoring in telecommunications engineering from Institut Teknologi Bandung, Indonesia, in 2018. He currently serves as a lecturer at the technology and vocational education faculty, Universitas Pendidikan Indonesia, Bandung, Indonesia. He is involved in telecommunications field research. His recent interests include but are not limited to propagation channels (measurement, analysis, modelling), software-defined radio, wireless sensing, unsupervised and supervised machine learning, and radar systems. He can be contacted at email: nurulfahmi@upi.edu.



**Mariya Al Qibtiya**    is a lecturer at the Faculty of Technical and Vocational Education (FPTK), Universitas Pendidikan Indonesia (UPI). In 2013 she received her bachelor's degree in Physics from Universitas Pendidikan Indonesia and master's degree in physics engineering from Institut Teknologi Bandung (ITB) in 2016. She has published some of academic research papers in several topics such as theoretical study and synthesis of solar cell and sensor materials, IoT, and machine learning. She is a member of the Institution of Electrical and Electronics Engineer (IEEE) from 2022. She can be contacted at email: mariyalqibtiya@upi.edu.